# Breaking the Backbone: Central Arginine Residues Induce Membrane Exit and Helix Distortions within a Dynamic Membrane Peptide

Matthew J. McKay,*[,†] Riqiang Fu,[‡] Denise V. Greathouse,[†] and Roger E. Koeppe, II[†]

[†]Department of Chemistry and Biochemistry, University of Arkansas, Fayetteville, Arkansas 72701, United States

[‡]National High Magnetic Field Laboratory, Florida State University, Tallahassee, Florida 32310, United States

S *Supporting Information*

ABSTRACT: Transmembrane domains of membrane proteins sometimes contain conserved charged or ionizable residues which may be essential for protein function and regulation. This work examines the molecular interactions of single Arg residues within a highly dynamic transmembrane peptide helix. To this end, we have modified the $GW^{4,20}ALP23$ (acetyl-GGA-$W^4(AL)_7AW^{20}AGA$-amide) model peptide framework to incorporate Arg residues near the center of the peptide. Peptide helix formation, orientation and dynamics were analyzed by means of solid-state NMR spectroscopy to monitor specific ^2H- or ^{15}N-labeled residues. $GW^{4,20}ALP23$ itself adopts a tilted orientation within lipid bilayer membranes. Nevertheless, the $GW^{4,20}ALP23$ helix exhibits moderate to high dynamic averaging of NMR observables, such as ^2H quadrupolar splittings or $^{15}N-^1H$ dipolar couplings, due to competition between the interfacial Trp residues on opposing helix faces. Here we examine how the helix dynamics are impacted by the introduction of a single Arg residue at position 12 or 14. Residue R14 restricts the helix to low dynamic averaging and a well-defined tilt that varies inversely with the lipid bilayer thickness. To compensate for the dominance of R14, the competing Trp residues cause partial unwinding of the helix at the C-terminal. By contrast, $R^{12}GW^{4,20}ALP23$ exits the DOPC bilayer to an interfacial surface-bound location. Interestingly, multiple orientations are exhibited by a single residue, Ala-9. Quadrupolar splittings generated by ^2H-labeled residues A3, A5, A7, and A9 do not fit to the α-helical quadrupolar wave plot defined by residues A11, A13, A15, A17, A19, and A21. The discontinuity at residue A9 implicates a helical swivel distortion and an apparent 3_{10}-helix involving the N-terminal residues preceding A11. These molecular features suggest that, while arginine residues are prominent factors controlling transmembrane helix dynamics, the influence of interfacial tryptophan residues cannot be ignored.
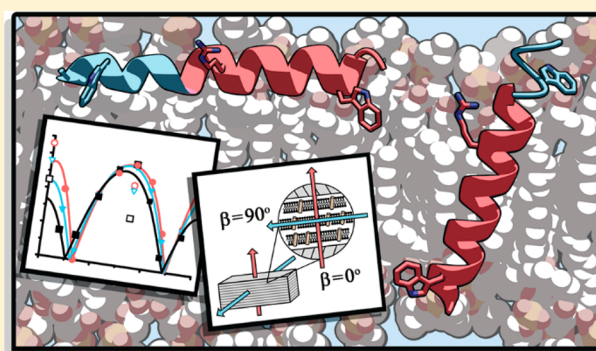
INTRODUCTION

Lipid-bilayer membranes define regions of high dielectric gradient. Indeed, by contrast with a lipid membrane surface, the nonpolar interior environment created by the acyl chains of a lipid bilayer is not readily hospitable for ionizable amino acid residues in membrane proteins. Nevertheless, the transmembrane domains of proteins sometimes contain noteworthy polar or charged residues which may be conserved and essential for protein function and regulation of cellular activity. For example, arginine residues play major roles in membrane voltage sensing domains of voltage-gated ion channels.[1,2] A "snorkeling" of positively charged arginine or lysine side chains to "reach" and interact with the lipid/membrane interface would help to keep the remaining nonpolar transmembrane domain within the hydrophobic membrane.[3,4] Direct evidence for snorkeling comes from NMR measurements of the $^{13}C-^{31}P$ distances for the Arg $C_α$ and $C_ζ$ carbons.[5,6] While notable snorkeling is observed for arginines in the voltage-sensing S4 helix of potassium channels,[6] it is not necessarily observed for

some antimicrobial peptides.[5] Nevertheless, in this regard, mutations that introduce polar and charged residues within transmembrane domains may have serious consequences affecting protein structure, function, and stability.

Due to numerous experimental challenges with large membrane proteins, simplified model systems can be useful for understanding the physical chemistry of the lipid interactions of ionizable protein side chains. The membrane-spanning peptide $GW^{5,19}ALP23$ (acetyl-$GGALW^5(LA)_6LW^{19}LAGA$-amide),[7] for example, has been useful for defining the titration properties of membrane-imbedded ionizable Arg, Lys, His, and Glu residues.[8−10a] $GW^{5,19}ALP23$ is advantageous because its robust helix adopts a well-defined orientation within lipid bilayers, wherein the helix tilt is dependent on membrane acyl chain length.[11] The chain

length dependence is likely a result of helix adaptation to the lipid-peptide hydrophobic mismatch.[11−13] Within this framework, specific arginine substitutions introduce new and interesting interactions between the peptide helix and its lipid environment.[14] Arg at position 14, for example, changes the tilt, forces a large helix rotation, and prefers to "snorkel", moving its side chain guanidium group into the bilayer lipid headgroup region. Molecular dynamics simulations additionally predict that the helix movement is accompanied by local membrane thinning.[14] By contrast, Arg placed at the dead-center of the GW^{5,19}ALP23 helix, at position 12, causes the helix to adopt multiple states. In DOPC membranes, both coarse-grained molecular simulations and solid-state NMR experiments predict the presence of three major states.[14] Two states retain a transmembrane helix with the arginine side chain "snorkeling" either "up" or "down" toward the polar lipid head groups. The third state is entirely different, with the complete helix exiting the lipid bilayer to adopt an interfacial orientation, perpendicular to the membrane normal. Modest amounts of cholesterol, about 10 mol %, in the DOPC membrane force essentially the entire R^{12}GW^{5,19}ALP23 population into this interfacial state.[15] The multistate features and membrane-exit property of R^{12}GW^{5,19}ALP23 are likely dictated by a Trp "cage" surrounding the R12 guanidium group, which effectively is trapped between the two aromatic side chains and restricted from favorable interactions with the bilayer head groups. Moving the Trp residues outward, to positions 3 and 21, increases the size of this cage and effectively frees the Arg side chain (at both positions 12 and 14) to permit a stable transmembrane orientation.[16]

Single transmembrane model helices reveal significant biophysical features for larger membrane proteins and are especially important for understanding (a) single-span membrane proteins[17−19] and (b) polar or charged functional groups that are in direct contact with the lipids.[5,8,14,20] Limitations arise when the interhelix protein−protein structural interactions in multihelix bundles[21,22] are not represented by the individual helices considered here. Nevertheless, the molecular features that underlie protein−lipid interactions, individual helix stability, and dynamics are well represented.[23,24]

Solid-state NMR methods are useful for examining transmembrane helices. For example, the pattern for the ^{2}H quadrupolar splittings of labeled Ala side chains around a helix can reveal the helix orientation and dynamics in a bilayer membrane.[25−28] In parallel fashion, the ^{1}H−^{15}N dipolar coupling and ^{15}N chemical shifts from labeled peptide backbone groups, observed in separated local field experiments,[29,30] also reveal the helix orientation and dynamics. The separated local field methods, in particular, have been applied to membrane proteins,[31,32] including the Vpu domain from HIV-1,[33] the chemokine receptor CXCR1,[34] phospholamban,[35] cytochrome P450 reductase,[36] cytochrome b5[37] and cytochrome P450,[38] individually and in complex,[18,39] the influenza A M2 proton channel,[40] and cell division regulatory protein CrgA,[41] among others.

Recently, we developed a highly dynamic peptide framework by relocating the Trp residues of GW^{5,19}ALP23 outward by only one sequence position on each side. With the Trp residues in positions 4 and 20, the large indole side chains then reside on opposite faces (Figure 1) of the α-helix of acetyl-GGAW^4(AL)$_7$AW^{20}AGA-amide.[42] The GW^{4,20}ALP23 helix experiences moderate to high motional averaging of solid-
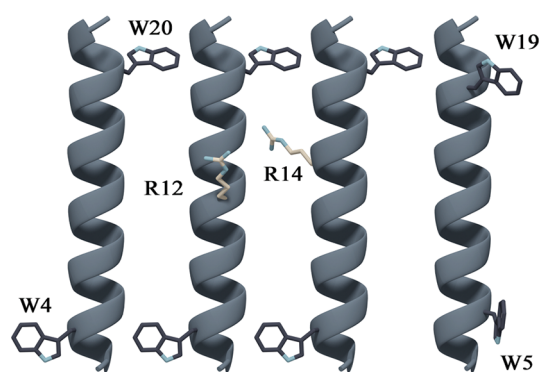

Figure 1. GWALP-like peptide models. From left to right: GW^{4,20}ALP23, R^{12}GW^{4,20}ALP23, R^{14}GW^{4,20}ALP23, and GW^{5,19}ALP23. See Table 1 for the amino acid sequences. While not depicted here, the helix terminals tend to fray.

state NMR observables such as ^{2}H quadrupolar splittings, ^{1}H−^{15}N dipolar couplings and ^{15}N chemical shifts. The excess dynamic averaging, much more than observed for GW^{5,19}ALP23, is caused primarily by additional rotation about the helix axis. The observed azimuthal slippage is attributed tentatively to a competition between the two Trp indole rings for preferential locations at the bilayer interface. An added benefit of the GW^{4,20}ALP23 sequence (Table 1) is

Table 1. Sequences of Arginine Containing GW^{4,20}ALP23 and GW^{5,19}ALP Peptides

name	sequence	ref
GW^{4,20}ALP23	acetyl-GGAW^{4}ALALALALALALALAW^{20}AGA-amide	42
R^{12}GW^{4,20}ALP23	acetyl-GGAW^{4}ALALALA**R**ALALALAW^{20}AGA-amide	this work
R^{14}GW^{4,20}ALP23	acetyl-GGAW^{4}ALALALALA**R**ALALAW^{20}AGA-amide	this work
GW^{5,19}ALP23	acetyl-GGALW^{5}LALALALALALALW^{19}LAGA-amide	7
R^{12}GW^{5,19}ALP23	acetyl-GGALW^{5}LALALA**R**ALALALW^{19}LAGA-amide	14
R^{14}GW^{5,19}ALP23	acetyl-GGALW^{5}LALALALA**R**ALALW^{19}LAGA-amide	14

the availability of two additional Ala residues for deuterium labeling, such that more ^{2}H are available for analysis of the α-helical structural perturbations. We take advantage of these features to examine the influence of single arginine substitutions in GW^{4,20}ALP23 (Table 1).

In this paper, we present the unique outcomes that result from introducing a central Arg residue into the dynamic GW^{4,20}ALP23 framework at position 12 or 14. Arginine at either position is situated on a different helix face from those of either Trp residue (Figures 1-2). Thus, neither R12 nor R14 in GW^{4,20}ALP23 is likely to fall within a Trp "cage". Nevertheless, the results will indicate that the R12 and R14 substitutions confer quite different modulations of the helix properties, with R12 not only driving the helix to the surface of DOPC membranes but also distorting the structure of the surface-bound helix. The results are significant for considering the complexity of arginine-guided rearrangements in membrane proteins, for example in response to specific mutations,[43,44] transmembrane voltages[44−46] or defects in arginine transport.[47]
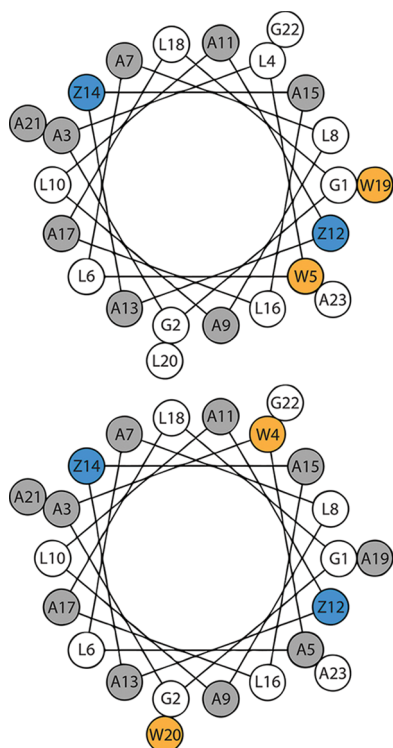
Figure 2. Helical wheel plots for GWALP-like peptides highlighting the Trp (W) locations with respect to residues 12 and 14. Top: GW^{5,19}ALP23; bottom: GW^{4,20}ALP23. Ala residues used for ^{2}H-labeling are depicted in gray. Trp residues are shown in yellow. Positions Z12 and Z14 (blue) are either Leu or one of them is substituted with Arg.

◼ METHODS

Materials. Fmoc-amino acids with protected side chains were purchased from Novabiochem (San Diego, CA). The tryptophan and arginine side chains were protected with *t*-butoxycarbonyl and 2,2,4,6,7-pentamethyldihydrobenzofuran-5-sulfonyl protecting groups, respectively. Commercial fmoc-L-alanine-^{15}N and fmoc-L-leucine-^{15}N were purchased from Cambridge Isotope Laboratories (Andover, MA). Commercial L-alanine-d_4 was also purchased from Cambridge Isotope Laboratories (Andover, MA) and was modified with an Fmoc group on a 100 mg scale as described.[48] Fmoc-L-alanine-d_4 was recrystallized from 20 mL ethyl acetate:hexane 80:20 and successful synthesis was confirmed using ^{1}H NMR. DLPC, DMPC, and DOPC lipids were purchased from Avanti Polar Lipids (Alabaster, Alabama). Other solvents and chemicals were the highest grade available.

Peptide Synthesis. Peptides R^{12}GW^{4,20}ALP23 and R^{14}GW^{4,20}ALP23 (see Table 1) were synthesized on a 0.1 mmol scale using solid-phase FastMoc chemistry[9] on a model 433A Applied Biosystems peptide synthesizer (Life Technologies, Foster City, CA). In most cases, two ala-d_4 residues were incorporated into each peptide in different isotopic abundances. In certain cases where spectral assignments remained ambiguous, a single ^{2}H-labeled alanine residue was used instead. ^{15}N-labeled peptides were also synthesized, containing two or three ^{15}N-labeled Ala or Leu residues. The peptides were purified on a Zorbax 300SB-C3 column (9.4 × 250 mm, 5-μm particle size; Agilent Technologies, Santa Clara, CA) with a gradient of 86−90% methanol (with 0.1% trifluoroacetic acid) over 11 min (R^{12}GW^{4,20}ALP23) or 13

min (R^{14}GW^{4,20}ALP23). MALDI mass spectrometry and analytical HPLC were used to confirm peptide identity and peptide purity of at least 95% (see Figure S1). Minor impurities were not characterized and will not affect the NMR spectra.

Circular Dichroism Experiments. Circular dichroism (CD) spectroscopy samples were prepared to analyze peptide helicity by using a 1:60 peptide:lipid mixture (62.5 nmol peptide and 3.75 μmol lipid). To prepare lipid vesicles, the samples were sonicated at 22 °C. The samples were analyzed using a Jasco (Easton, MD) J-1500 CD/Fluorescence spectropolarimeter with a 1 mm cell path, 1.0 nm bandwidth, 0.1 mm slit, and a scan speed of 20 nm/min, with averaging of 10 scans. CD-based estimates of the overall helix content were obtained from the CONTIN-LL and K2D programs implemented on the DICHROWEB online server.[49,50]

^{2}H Solid-State NMR Experiments. Mechanically aligned solid-state NMR samples were prepared by adaptations of previous procedures.[9,25,51,52] A peptide:lipid mixture having a ratio of 1:60 (1.33 μmol/80 μmol) was dispersed over about 40 thin glass plates and hydrated to 45% hydration (w/w) using deuterium-depleted water from Cambridge Isotope Laboratories (Andover, MA). Bilayer alignment in the sealed samples was confirmed using ^{31}P NMR at 121.5 MHz on a Bruker (Billerica, MA) Avance 300 spectrometer with broadband ^{1}H decoupling (4.2 kHz) for samples oriented at both β = 90° (bilayer normal perpendicular to the magnetic field) and β = 0° (see Figure S2). Solid-state ^{2}H NMR experiments were performed with a quadrupole-echo pulse sequence, with full phase cycling,[53] at 50 °C using a Bruker Avance 300 spectrometer at both sample orientations. The pulse sequence included a pulse time of 3.0 μs, an echo delay of 105 μs, and a recycle delay of 120 ms. Each ^{2}H NMR spectrum was acquired using 0.8 to 1.5 million scans. Based on measurements of two or more duplicate samples, an experimental uncertainty of ±1 kHz was estimated for the ^{2}H quadrupolar splittings.

^{15}N−^{1}H Dipolar Coupling/^{15}N Shift Solid-State NMR Experiments. Static solid-state NMR samples were prepared as described previously[9] using glass slides with dimensions measuring 5.7 × 10 mm NO. 000 purchased from Matsunami Glass (Bellingham, WA) and glass cells with dimensions measuring 5.4 × 7.4 × 18 mm purchased from New Era Enterprises (Vineland, NJ). Samples contained 1.33 μmol labeled peptide and 80 μmol lipid (1:60) and were hydrated to 45% (w/w) using deuterium depleted water.

Using a selective averaging "magic" polarization index ("SAMPI4") method,[54] separated local field spectra were recorded on a Bruker Avance NEO 600 MHz NMR spectrometer with Larmor frequencies of 600.13 and 60.81 MHz for ^{1}H and ^{15}N, respectively, using a low electrical field static 1H-X probe with a flat-coil configuration[55] with 1600 scans, 32 t1 increments, and a recycle delay of 4.0 s at 50 °C. The t1 evolution was preceded by Cross-Polarization with Mismatch-Optimized IS Transfer[56] with a contact time of 810 μs during which the radio frequency (RF) spin-lock amplitude of 50 kHz was used in both ^{1}H and ^{15}N RF channels. The SPINAL-64[17] decoupling sequence with the ^{1}H RF amplitude of 62.5 kHz was applied for ^{1}H heteronuclear decoupling during the 15 ms acquisition time.[57] The ^{1}H carrier frequency of 9 ppm was used and is optimal for transmembrane helices in oriented bilayers. The ^{15}N NMR data were processed and displayed using NMRPipe/NMRDraw[58] and Sparky[59] and
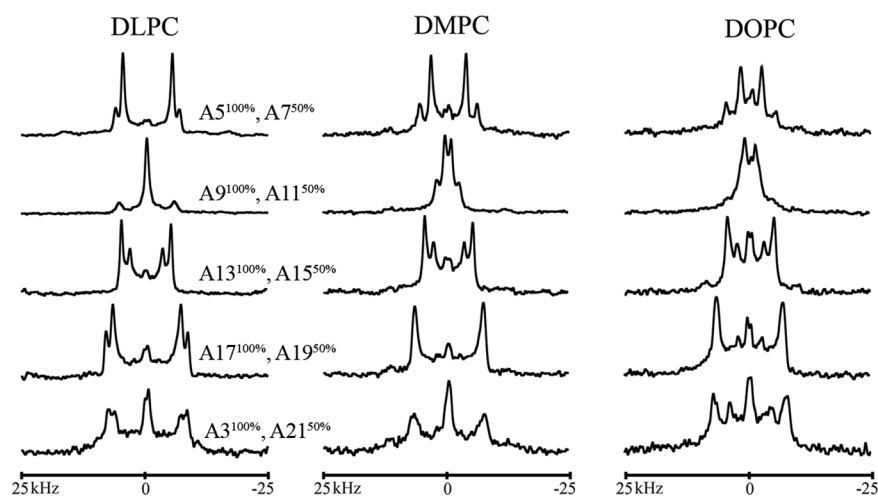
Figure 3. ^{2}H NMR spectra for labeled alanines of R^{14}GW^{4,20}ALP23 in mechanically aligned DLPC, DMPC, and DOPC bilayers. Samples consisted of 1.3 μmol peptide with 80 μmol lipid oriented at β = 90°, temperature 50 °C. Between 0.8 and 1.5 million scans were acquired during 25−50 h. The sequence numbers of the ^{2}H-labeled alanines are from top to bottom (5$^{100\%}$, 7$^{50\%}$); (9, 11); (13, 15); (17, 19); and (3, 21). The first alanine of each pair is 100% deuterated while the second is 50% deuterated.

adjusted using the theoretical dipolar coupling scaling factor for SAMPI4 evolution.[54] The ^{15}N chemical shifts were externally referenced to ^{15}N-labeled solid ammonium sulfate, set to 26.8 ppm, corresponding to the signal from liquid ammonia at 0 ppm.[60]

Data Analysis. Analysis of the ^{2}H NMR spectra was performed using the semistatic geometric analysis of labeled alanines (GALA) as described previously by van der Wel et al. 2002.[25] The deuterium quadrupolar splittings of the alanine methyl groups ($\Delta\nu_q$) are dependent on the macroscopic sample orientation as seen in eq 1 below.

$$\Delta\nu_q = \text{QCC} \times S_{zz} \times \left[\frac{1}{2}(3\cos^2\theta - 1)\right]\left[\frac{1}{2}(3\cos^2\beta - 1)\right]$$
$$\left\langle\frac{1}{2}(3\cos^2\gamma - 1)\right\rangle \tag{1}$$

Known constants within this equation include the angle between the membrane normal and the applied magnetic field (β) = 90° or 0°, the quadrupolar coupling constant for an aliphatic C−D bond (QCC) = 168 kHz, and the tetrahedral bond angle of the CD$_3$ group (γ) = 109.5° which results in a 1/3 reduction of the coupling constant due to the fast rotation of the methyl group. This leaves the principal order parameter S$_{zz}$, which serves as an estimate for peptide motion, and θ, the angle between the magnetic field and the C$_\alpha$-C$_\beta$ bond of the alanine side chain, as variables. The θ angle, in turn, is dependent on the average peptide orientation as seen in eq 2 below.

$$\theta = \varepsilon_\parallel[\cos\tau_0 - \sin\tau_0 \cos(\rho_0 + \varepsilon_\perp + \varphi)\tan\varepsilon_\parallel] \tag{2}$$

The angles defining the local side chain orientation with respect to the C$_\alpha$-C$_\beta$ bond ($\varepsilon_\parallel$) and a plane perpendicular to the helix direction ($\varepsilon_\perp$) are fixed to +59.4° and −43.3° respectively, as determined previously.[25] The angle φ is the angle between a reference point (here C$_\alpha$ of Gly^1)[25] and C$_\alpha$ of the deuterium labeled residue in the peptide.

The GALA method, therefore, considers an α-helical geometry and three adjustable parameters: the apparent tilt τ_0 of the helix axis with respect to the bilayer normal, the helix azimuthal rotation ρ_0 and the order parameter S$_{zz}$ (eq 1 and eq

2).[25] The GALA calculation finds the lowest RMSD fit between the experimental $\Delta\nu_q$'s and those calculated for the peptide helix as it samples available orientations with respect to the bilayer normal and the reference point for φ. Deviations from α-helical geometry result in either a uniformly high global RMSD or individual data points deviating from the GALA quadrupolar wave.[10] For our analysis, we searched ranges of τ_0 (0−90°) and ρ_0 (0−359°), each incremented by steps of 1°, and S$_{zz}$ (0−1.0) by steps of 0.1.

To modify the GALA calculation to match the ^{2}H NMR data to a 3$_{10}$ helix instead of an α-helix, the calculation for the angle φ was changed by modifying η, the helical wheel separation between the residue in question (n) and the previous residue ($n - 1$) in eq 3 below. For a canonical α-helix η = 100°, and for a canonical 3$_{10}$-helix η = 120°.

$$\varphi = (n - 1) \times \eta + 360 \tag{3}$$

A canonical 3$_{10}$-helix with η = 120° would result in every third Ala residue generating, predictably, the same ^{2}H-methyl quadrupolar splitting, which was not observed in this study. The value of η = 120° also is unreasonable because of side chain repulsion between residue n and residue (n+3). Instead, average 3$_{10}$-helix torsion angles (−71°, −18° for ϕ, ψ) found in nature were used resulting in η = 112.5°.[61] This value of η also results in $\varepsilon_\parallel$ of 61° and $\varepsilon_\perp$ of −38° required for eq 2 above. The angles $\varepsilon_\parallel$ and $\varepsilon_\perp$ were calculated using a combination of UCSF Chimera and Blender (open-source 3D graphics software).[62,63]

The availability of eight core alanine residues in GW^{4,20}ALP23 is especially useful when studying peptides that exhibit increased dynamic motion.[42,64] The large data pool allows for a more demanding Gaussian analysis to be utilized over ^{2}H quadrupolar splittings individually or combined with ^{15}N chemical shifts and ^{15}N/^{1}H dipolar couplings, as derived from model 6 of Strandberg et al, 2009.[65] This model of helix dynamics considers a Gaussian distribution of helix tilt τ and rotation ρ angles centered at the angles τ_0 and ρ_0 with widths as the oscillations about them, σ_τ (helix wobble) and σ_ρ (rotational slippage) respectively. The calculation performs a grid search over the variables τ_0, ρ_0 and their standard deviations σ_τ and σ_ρ, while fixing a principal order parameter

Table 2. Quadrupolar Splitting Magnitudes ($|\Delta\nu_q|$, in kHz) for Labeled Alanine CD_3 Groups in $R^{14}GW^{4,20}ALP23$ and $R^{12}GW^{4,20}ALP23^a$

	$R^{14}GW^{4,20}ALP23$ alanine CD_3 position/$\Delta\nu q$ (kHz)									
Lipid	3	5	7	9	11	13	15	17	19	21
DLPC	30.0	20.2	25.8	0.1	11.2	20.0	13.2	27.0	33.0	24.0
DMPC	29.4	14.2	23.2	2.6	8.8	19.7	12.5	28.0	28.0	24.0
DOPC	30.2	8.2	20.1	7.3	4.1	19.3	10.8	28.1	22.4	14.3
	$R^{12}GW^{4,20}ALP23$ Alanine CD_3 Position/$\Delta\nu q$ (kHz)									
Lipid	**3**	**5**	**7**	**9(a)/(b)**	**11**	**13**	**15**	**17**	**19**	**21**
DOPC	18.9	0.5	23.2	27.4/11.4	21.0	0.7	13.2	37.1	25.0	31.0

$^a\beta = 0°$ sample orientation. The measurement uncertainty is ±1 kHz. ^{b}Residue A9 gives two signals in DOPC, designated as 9a (27.4 kHz) and 9b (11.4 kHz).

S_{zz} to either 1.0 (no isotropic motion) or 0.88 as an estimate for the isotropic internal motion of a transmembrane peptide, or another value. Our analysis was performed by varying, in 1° increments, τ_0 from 0° to 90°, ρ_0 from 0° to 359°, σ_τ from 0° to 30° and σ_ρ from 0° to 200°. In cases of a limited availability of data points, a modified Gaussian calculation was used instead by restraining σ_τ to a small finite value and varying the remaining three parameters as above. The in-house program estimates the helical geometry based on a polyalanine α-helix model. Modifying the torsion angles within the model allows the data to be fit to a tighter 3_{10}-helix. The α-helix torsion angles for ϕ and ψ ($-64°$ and $-40°$)[66] were modified to $-71°$ and $-18°$, respectively, to represent a 3_{10} helix, based on the mean torsion angles found within naturally occurring 3_{10}-helices.[61]

In cases of helix distortion, the peptide kink angle (κ) can be calculated using eq 4 below with the rotation (ρ) and tilt (τ) relative to either the C-terminal or N-terminal segment of the peptide helix.[67]

$$\cos \kappa = \sin(\tau_N) \sin(\tau_C) \cos(\Delta\rho) + \cos(\tau_N) \cos(\tau_C) \quad (4)$$

■ RESULTS

The parent peptide helix of $GW^{4,20}ALP23$ exhibits extensive dynamic averaging in lipid-bilayer membranes.[42] The present experiments reveal the influence of introducing a single charged Arg residue into this highly dynamic helical framework at position 14 or position 12 of the 23-residue sequence.

$R^{14}GW^{4,20}ALP23$. Solid-state NMR techniques have proven useful for determining the extent of a transmembrane peptide's helicity[24] and furthermore the helix average orientation and dynamics within its lipid environment. A key result is that the presence of R14 lowers dramatically the extent of motional averaging. The reduced motion is evident from the wide range of ^2H quadrupolar splittings, from 1 kHz to 33 kHz, observed for the collection of Ala methyl side chains in $R^{14}GW^{4,20}ALP23$ (Figures 3 and S3 and Table 2), compared to the narrow range of 1 kHz to 16 kHz when R14 is absent in $GW^{4,20}ALP23$.[42] For reference, a moderately dynamic peptide such as $GW^{5,19}ALP23$ produces core alanine ^2H quadrupolar splittings that span a range of about 1 kHz to 27 kHz.[11] Therefore, the presence of R14 indeed decreases the high extent of motional averaging of the ^2H NMR signals from the host peptide helix.

The helix orientations can be compared using the semistatic GALA method to analyze the patterns of alanine methyl ^2H quadrupolar splittings.[25] Indeed, the GALA quadrupolar wave-plots (Figure 4A) reveal a rather constant helix azimuthal rotation ρ_0 of ~224° (Table 3) for $R^{14}GW^{4,20}ALP23$ in DLPC, DMPC and DOPC bilayer membranes. An essentially constant
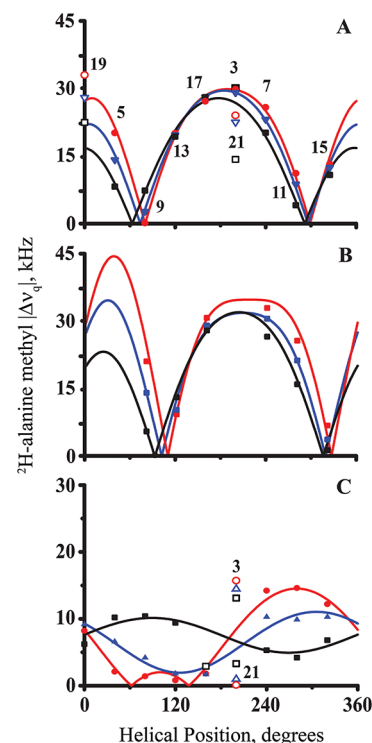

Figure 4. GALA quadrupolar wave plots for (A) $R^{14}GW^{4,20}ALP23$, (B) $R^{14}GW^{5,19}ALP23$, and (C) $GW^{4,20}ALP23$ in DLPC (red), DMPC (blue), and DOPC (black) bilayers. Data points with white filling were omitted from the analysis. The helix orientations corresponding to the quadrupolar waves are listed in Table 3.

preferred value of ρ_0, independent of the bilayer thickness, is indicative and even diagnostic of low dynamic averaging.[11,28] Hand in hand with the low dynamic averaging, the tilt τ_0 of the $R^{14}GW^{4,20}ALP23$ helix decreases systematically as the lipid bilayer thickness increases (τ_0 being 21°, 17°, and 14° in DLPC, DMPC, and DOPC, respectively). This behavior contrasts sharply with that of $GW^{4,20}ALP23$, which shows extensive variation for ρ_0 and no correlation for τ_0 with the lipid environment (Figure 4C). The arginine residue R14 has served to stabilize the membrane-incorporated helix in a preferred orientation.

The quadrupolar wave plots for $R^{14}GW^{4,20}ALP23$ are nicely similar to those of $R^{14}GW^{5,19}ALP23$, illustrating similar helix tilt angles and a difference of only 25° in the azimuthal rotation ρ_0 about the helix axis (Figure 4A,B). While it is apparent that the location of the Arg residue dominates the tilt in both peptides, the small difference in rotation is due to differences

Table 3. GALA and Gaussian Fits Using Ala-CD₃ $|\Delta\nu_q|$ Magnitudes of Arg-Containing GWALP23 Family Peptides[a]

lipid	peptide	GALA fit results				Gaussian fit results					ref
		τ_0	ρ_0	S_{zz}	RMSD	τ_0	ρ_0	$\sigma\rho$	$\sigma\tau$	RMSD	
DLPC	W[4,20]	6.0°	322°	0.72	0.70	16°	321°	85°	15°	0.49	42
	W[5,19]	20.7°	305°	0.71	0.66	23°	304°	33°	5°[b]	0.70	42
	R[14]W[4,20]	21.3°	223°	0.77	0.92	21°	223°	24°	14°	0.74	this work
	R[14]W[5,19]	30.0°	259°	0.83	1.58	30°	260°	<10°	5°[b]	1.65	14; this work
DMPC	W[4,20]	3.3°	349°	0.71	0.85	5°	347°	51°	20°	0.68	42
	W[5,19]	11.7°	311°	0.87	0.90	13°	308°	44°	5°[b]	1.10	42
	R[14]W[4,20]	16.7°	228°	0.85	0.75	17°	228°	12°	6°	0.72	this work
	R[14]W[5,19]	25.8°	252°	0.81	1.59	26°	252°	28°	5°[b]	0.97	14; this work
DOPC	W[4,20]	1.7°	133°	0.81	0.80	9°	129°	122°	5°	0.78	42
	W[5,19]	6.0°	323°	0.87	0.60	9°	321°	48°	5°[b]	0.70	42
	R[14]W[4,20]	13.3°	221°	0.90	0.81	14°	220°	9°	2°	0.87	this work
	R[14]W[5,19]	16.1°	246°	0.94	1.29	16°	246°	<10°	5°[b]	1.20	14; this work

[a]The abbreviations refer to peptides based on the locations of selected aromatic residues, W[4,20] in GW[4,20]ALP23 and W[5,19] in GW[5,19]ALP23, with or without arginine R14, as noted. See also Table 1. The uncertainties in τ_0 and ρ_0 are about 2° and 5°, respectfully. The widths of the distributions around τ_0 and ρ_0 are given by $\sigma\tau$ and $\sigma\rho$. [b]A modified three variable Gaussian treatment[28,93] was used to analyze the six core Ala-CD₃ data points constraining $\sigma\tau$ to 5°.

in the locations of the interfacial tryptophans, W[4,20] as opposed to W[5,19]. Interestingly, residues A19 and A21 of R[14]GW[4,20]ALP23 fall off their respective curves for the core helix in all three lipids, whereas A3 fits in all three cases (Figure 4A). These features imply more extensive fraying of the helix at the C-terminal as opposed to the N-terminal.[10b,23] The circular dichroism spectra (Figure 5A) show differences in the ε_{222} to
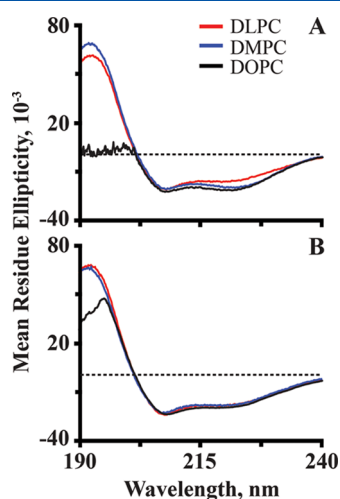

Figure 5. Circular dichroism spectra for (A) R[14]GW[4,20]ALP23 and (B) R[12]GW[4,20]ALP23 in lipid vesicles. The dotted black lines indicate where the mean residue ellipticity is zero. The DOPC double bond absorbs below 200 nm and is responsible for the distortion shown.

ε_{208} ratio in several lipid vesicles, which may be due to small lipid-dependent changes in helix backbone structure. Analysis using the CONTIN-LL program based on ridge regression,[68,69] available on the DICHROWEB online server,[49,50] gave estimates of 66% helix in DLPC, 67% in DMPC, and 54% in DOPC. Analysis using an alternative method K2D[70] gave comparable estimates of 57% helix in DLPC, 69% in DMPC, and 77% in DOPC. Notably, the NMR results indicate an incomplete helix from which residues 19−23 are unraveled in each lipid membrane. Differing side-chain torsion angles for the indole rings also could raise uncertainty about the CD estimates of the backbone helicity.[71]

A Gaussian analysis of the ²H quadrupolar splittings[27,28,65] provides further insight into the dynamics of the R[14]GW[4,20]ALP23 helix, in particular the lowering of the rotational slippage about the helix axis (σ_ρ). As seen in Table 3, with R14 present, σ_ρ drops from a large value to less than 25° in all three lipids. These values are not only significantly less than those of GW[4,20]ALP23, but are also lower than those observed for the parent GW[5,19]ALP23 helix. Indeed, a single arginine residue generally dictates a preferred helix rotation ρ_0 and lowers the width of the distribution σ_ρ about ρ_0.[64] The strikingly low extent of rotational slippage exhibited by R[14]GW[4,20]ALP23 implies that the mere presence of R14 is enough to restrict the host peptide helix to minimal amounts of motional averaging.

R[12]GW[4,20]ALP23. In the framework of GW[5,19]ALP23, an introduction of R12 leads to multiple states for the helix.[14] In similar fashion, in the framework of GW[4,20]ALP23, at least one residue, A9, exhibits two states (Figure 6; see also Figure S4). Do the two different quadrupolar splittings of 11.4 kHz and 27.4 kHz (Table 2) for residue A9 in R[12]GW[4,20]ALP23 reflect global changes for the entire molecule or local structural plasticity near residue A9? We note in this case that local variations are more likely because only residue A9, and
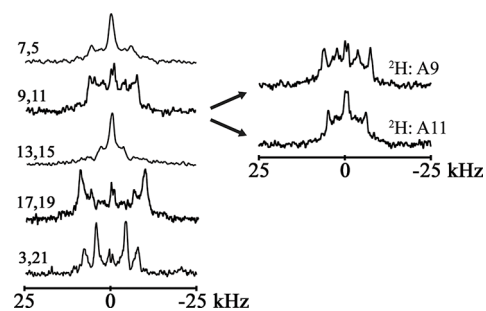

Figure 6. ²H NMR spectra for labeled alanines R[12]GW[4,20]ALP23 in mechanically aligned DOPC bilayers. Samples consisted of 1.3 μmol peptide with 80 μmol lipid oriented at $\beta = 90°$, temperature 50 °C. Between 0.8 and 1.5 million scans were acquired during 25−50 h. The label positions and % deuteration are from top to bottom: (A5[100%], A7[50%]); (A9[100%], A11[50%]); (A13[100%], A15[50%]); (A17[100%], A19[50%]); and (A3[100%], A21[50%]).

Table 4. $R^{12}GW^{4,20}ALP23$ Structure, Orientation, and Dynamics at the Surface of DOPC Bilayers[a]

	C-terminus					N-terminus				
α-helix	τ_0	ρ_0	$\sigma\rho$	$\sigma\tau$	RMSD	τ_0	ρ_0	$\sigma\rho$	$\sigma\tau$	RMSD
^2H	83°	31°	12°	28°	1.28[b]	no fit				
$^{15}N,^1H/^{15}N$	87°	42°	25°	5°	0.69	88°	178°	44°	7°	0.89
combined	84°	34°	22°	5°	0.86	no fit				
3_{10}-helix[c]										
^2H	no fit					85°	353°	27°	30°	0.66[d]
$^{15}N,^1H/^{15}N$	86°	22°	42°	5°	0.66	88°	348°	48°	7°	0.74
combined	no fit					85°	349°	29°	27°	1.22

[a]The N-terminal fits were calculated using ^2H resonances for residues A3, A5, A7, A9b, and A11, or $^1H/^{15}N$ observables for residues A5, L6, A7, L8, A9b. The C-terminal data points included ^2H quadrupolar splittings for residues A9a, A11, A13, A15, A17, A19, or $^1H/^{15}N$ observables for residues A9a, A13, L14, A15, L16, and A17. The combined fits used the ^2H quadrupolar splittings together with the indicated $^1H/^{15}N$ observables. For these surface helices, the uncertainties in τ_0 and ρ_0 are about 2°. The widths of the distributions around τ_0 and ρ_0 are given by $\sigma\tau$ and $\sigma\rho$. [b]For comparison with the Gaussian fit for the ^2H data to the C-terminal α-helix, a semistatic GALA analysis gave $\tau_0 = 86°$ $\rho_0 = 33°$, S_{zz} of 0.64 and RMSD of 1.25 kHz. [c]The results suggest that the $^{15}N/^1H$ results could fit either an α-helix or a similarly oriented 3_{10}-helix for either segment (N-terminal or C-terminal), with in all cases a significant discontinuity (change in azimuthal rotation ρ_0) at residue 9. The ^2H results, by contrast, show distinct preferences of an α-helix for the C-terminus and a 3_{10}-helix for the N-terminus. The ^2H quadrupolar splitting is highly sensitive to the local bond orientation. [d]For comparison, a semistatic GALA analysis gave $\tau_0 = 86°$, $\rho_0 = 3°$, S_{zz} of 0.51 and RMSD of 0.47 kHz.

possibly A11, exhibits multiple ^2H NMR peaks (Figure 6). (Only one state can easily be resolved for A11; see the Discussion.) This contrasts with the behavior of $R^{12}GW^{5,19}ALP23$ which shows three states for the global helix in DOPC and generates multiple ^2H NMR peaks for every Ala residue.[14] The range of observed ^2H-Ala quadrupolar splittings (0.5 to 37 kHz; see Table 2) also is higher for $R^{12}GW^{4,20}ALP23$ than for $R^{12}GW^{5,19}ALP23$.

To fit describe the orientation of the $R^{12}GW^{4,20}ALP23$ helix, a GALA or Gaussian fit (Table 4) describes a surface-bound α-helix for the C-terminal of the core sequence from residue A9(a) through A19. This α-helical segment is oriented with τ_0 of about 86° with respect to the bilayer normal, rotated such that $\rho_0 = 33°$, and fits with an RMSD of 1.25 kHz (Table 4) on the surface of a DOPC bilayer. Notably, the alternate configuration for alanine-9 (spectrally indicated by the ^2H NMR $|\Delta\nu_q|$ for A9(b); Figure 6 and Table 2) and the sole configurations for alanines 3, 5, and 7 do not fit the α-helix defined by the C-terminal segment (Figure 7A). Instead, the N-terminal segment fits a suitably analyzed 3_{10}-helix on the DOPC membrane surface.

From the CD spectra (Figure 5), the estimates of the helicity are lower for $R^{12}GW^{4,20}ALP23$ in DOPC than in thinner membranes, namely 37% in DOPC as opposed to 70% (DMPC) or 71% (DLPC), based on the CONTIN-LL method.[68,69] The K2D method[70] gave similar predictions of 31% in DOPC, 60% in DMPC and 65% in DLPC. Consistent with these CD predictions, notably, the NMR results (see below) indicate that a portion of the helix converts to a 3_{10} helix in DOPC.

While uncommon in typical transmembrane domains, the arginine rich voltage sensing domains of channel proteins are sometimes observed to contain 3_{10}-helix motifs;[72–74] see the Discussion. Modifying the GALA and Gaussian calculations to fit the N-terminal portion of the peptide to a tighter 3_{10}-helix yields interesting results that provide further insight. The canonical Pauling 3_{10}-helix with exactly 3.0 residues/turn[75] would not fit the experimental data, since every third residue would occupy the same position on a helical wheel and would therefore generate the same ^2H quadrupolar splitting, which is not the case here. In line with our observations, nevertheless, the average helical wheel residue separation in 3_{10}-helices
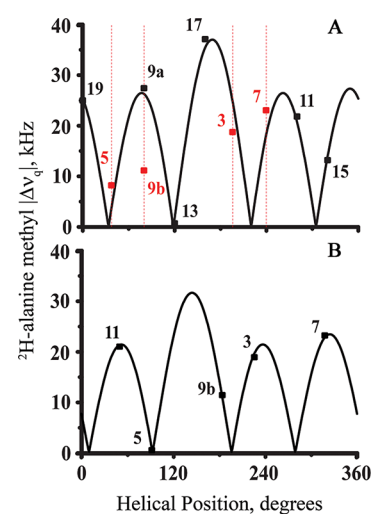

Figure 7. GALA quadrupolar wave plots for $R^{12}GW^{4,20}ALP23$ DOPC bilayers. (A) Wave plot for the C-terminal α-helix (τ_0 86°, ρ_0 33°), with data points for A9b, A7, A5, and A3 (red) not fitting the curve and omitted in the analysis used to generate the wave plot. (B) Wave plot for a 3_{10}-helix for the N-terminal (A3-A11 with A9b).

observed in nature is not 120° but rather is roughly 112.5°, which corresponds to about 3.2 residues/turn. We therefore used values of 112°−114° for the radial separation to model the solid-state NMR data for the N-terminal as a 3_{10}-helix.[61,76] When applied to the ^2H quadrupolar splittings (Table 2), or in combination with the ^{15}N data (see below), the best Gaussian and GALA fits predict a surface bound N-terminal 3_{10}-helical segment with 112.5° as the average residue radial separation, oriented with τ_0 of 85°−88°, ρ_0 around 350° and RMSD values between 0.5 and 0.9 kHz (Table 4). These N-terminal average tilt angles above 85° calculated for the tighter 3_{10}-helix are strikingly similar to the predicted surface orientation of the C-terminal α-helix. The discontinuity at residue A9, nevertheless, indicates an unwinding denoted by the 30°−40° difference in azimuthal rotation about the axes of the α- and 3_{10}-helices (Table 4; Figure 7). Notably, the ^2H NMR observables can only fit the C-terminal residues to an α-helix and the N-terminal residues to a tighter helix such as a 3_{10}-helix. For the N-terminal ^2H data, a modified Gaussian calculation (see[24])

was incorporated in order to obtain an estimate of the dynamics if fitted to a 3_{10}-helix. In this case, both $\sigma\rho$ and $\sigma\tau$ would be moderate (Table 4). Therefore, a tighter helix, such as a 3_{10}-helix, with likely varying torsion angles,[61,76] is a probable structure for the N-terminal portion of $R^{12}GW^{4,20}ALP23$ on the DOPC membrane surface.

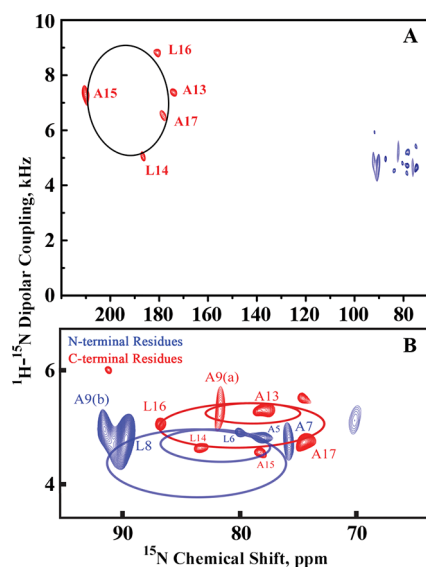The helix discontinuity was confirmed also with ^{15}N experiments (Figure 8). The spectra in Figure 8 were drawn

Figure 8. Separated local field ^{15}N spectra for a transmembrane helix and a distorted surface helix. A. The red peaks arise from resonances for selected ^{15}N backbone labels on transmembrane KWALP23 in static aligned DLPC bilayers oriented at $\beta = 0°$, with the ellipse representing a helix tiled 19° from the bilayer normal. The blue peaks arise from ^{15}N labels in $R^{12}GW^{4,20}ALP23$, bound to the surface of DOPC bilayers. B. Expansion and highlights for multiple selectively labeled $R^{12}GW^{4,20}ALP23$ peptides in static aligned DOPC bilayers (1.3 μmol peptide with 80 μmol lipid) oriented with $\beta = 0°$, 1400−1600 scans and temperature of 50 °C over ∼22 h. The PISA wheels shown are fitted to C-terminal residues (red, α-helix) and N-terminal residues (blue, 3_{10}-helix). See also Table 4. The assignments for ^{15}N backbone labels are shown.

from four differently labeled samples of $R^{12}GW^{4,20}ALP23$ and a control sample of KWALP23[11,64] to represent a prototype transmembrane helix. Sample variation led to differing signal intensities and signal-to-noise ratios. One-dimensional spectral slices in the dipolar coupling dimension are shown for each ^{15}N-labeled residue in Figure S5 of the Supporting Information. The ^{15}N NMR spectra indicate and confirm the surface orientation and the discontinuity at residue A9 for the $R^{12}GW^{4,20}ALP23$ helix. The ^2H and ^{15}N solid-state NMR experiments therefore agree. For example, the spectra obtained from the SAMPI4 experiments (Figure 8) have ^{15}N chemical shifts between 95 and 70 ppm as well as dipolar couplings between 4 and 6 kHz, which indicate a surface bound orientation,[77] perpendicular to the membrane normal, in contrast to the spectrum for a control transmembrane helix (Figure 8A). Residue A9 once again shows resonance doubling. Furthermore, the dipolar wave plot depicted in Figure 9 shows a discontinuity in frequency and amplitude of the dipolar wave at residue A9, as the patterns N-terminal and C-terminal to residue A9 are distinctly different, with a much larger amplitude for the wave C-terminal to alanine 9.
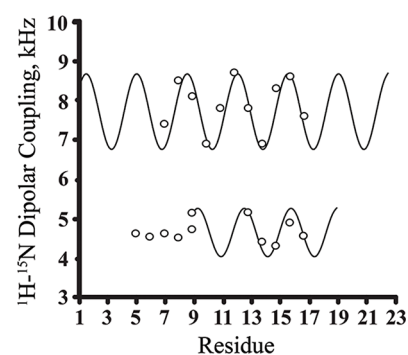

Figure 9. Dipolar waves depicting the static $^1H−^{15}N$ dipolar couplings as a function of residue position for transmembrane $GW^{5,19}ALP23$ in DLPC bilayers (top) adapted from ref 64 and surface bound $R^{12}GW^{4,20}ALP23$ in DOPC bilayers (bottom).

Supporting the ^{15}N dipolar wave, the expanded region of the two-dimensional SAMPI4 spectrum (Figure 8B) shows separate elliptical patterns for the C-terminal and N-terminal segments. The ^{15}N polarity index slant angle ("PISA") pattern in Figure 8B predicts a tilt τ_0 of 89° and a ρ_0 of 42° for the C-terminal residues (Table 4), in agreement with the ^2H NMR data. The small difference of 10° in the estimate for ρ_0 (Table 4) is likely due to the lower sensitivity of the SAMPI4 experiment, compared to the ^2H experiment, to the helix azimuthal rotation. Once again, the ^{15}N chemical shift range for the N-terminal residues indicates a surface-bound orientation for this portion of the helix (Figure 8).[78,79]

Gaussian analyses reported in Table 4 indicate that the ^{15}N NMR observables "could" fit the N- and C-terminal segments, with different ρ_0 values, to α-helical or 3_{10}-helical segments on the DOPC membrane surface. The ambiguity for the ^{15}N experiment is expected due to the similar locations of 90° tilted peptide 3_{10}-helix and α-helix PISA wheels.[76] The wheel positions are furthermore influenced by the extent of dynamic averaging.[18,37] Nevertheless, the ^2H quadrupolar splittings can fit the C-terminal residues only to an α-helix, and the N-terminal residues only to a 3_{10}-helix (see above). Additionally, only a 3_{10}-helix fits the ^{15}N data for the N-terminal if the extent of rotational slippage ($\sigma\rho$) is moderate ($\sigma\rho$ of 39−44°) instead of very high. A hypothetically higher $\sigma\rho$ would in turn lead to more signal averaging and "would" make feasible an N-terminal α-helix, with similar PISA wheel size as the blue wheel in Figure 8B. Altogether, nevertheless, the ^{15}N and ^2H NMR observables agree concerning the surface location for $R^{12}GW^{4,20}ALP23$, the rotational discontinuity of 30°−40° at residue A9, the C-terminal α-helix motif and the N-terminal 3_{10}-helix motif (Table 4).

■ DISCUSSION

Arginine dominates the GWALP23 peptide helix dynamics and behavior in a manner dependent on its location within the sequence relative to those of the juxta-terminal interfacial Trp residues. In the original $GW^{5,19}ALP23$ peptide, the presence of R14 on the opposite face of the helix from that occupied by the two Trp residues (Figure 2) allows the peptide to remain transmembrane in bilayers of DOPC, yet with a 10° increase in tilt and 80° change in helix azimuthal rotation.[14] By contrast, R12, more centrally located and effectively "trapped" within a Trp "cage" defined by W5 and W19, leads to multiple states for the helix, including two competing transmembrane orientations and one at the surface of DOPC bilayers.[14] The

multistate behavior can be "rescued" by moving the tryptophans outward to positions 3 and 21.[16] In the context of W3 and W21, arginine R12 as well as R14 can be accommodated in a suitably tilted transmembrane helix.[16] Toleration of R12 with W3 and W21 as opposed to W5 and W19 has been attributed to the guanidium group occupying a different helix face and no longer needing to compete with the Trp residues for favorable interactions at the interface. Interestingly, R14 also is accommodated with W3 and W21, perhaps because the Trp "cage" is effectively larger than that defined by W5 and W19.

For the present investigation, the structural context for W4 and W20 on the helix framework is entirely different. From this perspective, neither position 12 nor position 14 is located on a helix face containing a Trp residue. Therefore, while the two former cases ($W^{5,19}$ and $W^{3,21}$) have addressed primarily the possibility that Trp could restrict water access to a central Arg side chain, the $W^{4,20}$ sequence removes this side chain competition and introduces instead a new factor, high dynamic motion for the parent helix when no arginine is present. Indeed, the helix of $GW^{4,20}ALP23$ undergoes extensive motional averaging in the form of rotational slippage about the helix axis in order to compensate for apparently competing radial locations of the Trp residues and a rotation-dependent hydrophobic mismatch.[42] The inclusion of Arg at either position 12 or 14 within this sequence severely limits the excessive dynamic averaging and in each case leads to helix structural distortions, previously unobserved in the former $GW^{5,19}ALP23$ framework.

Importantly, the Arg side chain carries a positive charge under all conditions.[15,80] The finding is verified by numerous experimental and computational results.[15,81−84] Indeed, the solution pK_a for Arg has been revised upward to a value of 13.8,[80] and recent experiments showed that $R^{14}GW^{5,19}ALP23$ remains fully charged up to pH 13 within an ether-linked lipid environment.[15] Helix translocation, side chain snorkeling and membrane deformation can also serve to stabilize the positive charge, allowing the Arg side chain to engage in favorable interactions at the membrane interface.[14,85,86]

Influence of R14. The unmodified $GW^{5,19}ALP23$ helix already displayed a transmembrane orientation with low levels of dynamic averaging.[28] Incorporating R14 resulted in a 10° increase in tilt, 80° change in helix rotation and mean helix displacement/membrane thinning (observed via coarse grain simulations)[14] that allow the Arg to snorkel and access the membrane interface. The transmembrane orientations for the helices with $W^{5,19}$ and $W^{4,20}$ are similar, with low dynamic averaging for each, when R14 is present. The respective helix tilt angles differ by about 9° in DLPC and DMPC (Table 3) but by only about 3° in DOPC. The helix azimuthal rotation differs modestly by 25−36° when the Trp sequence context is changed with R14 present (see Table 3, Figure 4). The arginine residue R14 is therefore the primary determinant of the helix tilt and azimuthal rotation, but the interfacial Trp residues, whether W5 and W19 or W4 and W20, exert secondary influence for fine-tuning of the helix tilt and rotation. Residue R14 also lowers the extent of dynamic averaging, dramatically for the highly dynamic $GW^{4,20}ALP23$ helix, and much more modestly for the already low-averaging $GW^{5,19}ALP23$ helix.[64] The rotational slippage in the form of $\sigma\rho$ for both helices with R14 is remarkably low in all three lipids (<25°, Table 3), indeed lower than for $GW^{5,19}ALP23$ with arginine absent. Therefore, the single arginine residue governs

the overall properties of these transmembrane helices, with the small differences in the tilt and rotation due to the locations of the juxta-terminal Trp residues.

The dominance of arginine R14 over the peptide dynamics would also explain the helix unwinding observed at the C-terminal in $R^{14}GW^{4,20}ALP23$. The opposing radial positions of the distal tryptophans, W4 and W20, are responsible for the high dynamic motion exhibited by the host peptide. This arrangement causes the indole side chains to compete with one another for better positions at the lipid/water interface. Furthermore, as the helix cannot solely rely on adjusting its τ_0 and ρ_0 to satisfy hydrophobic mismatch, it additionally exhibits increased oscillations about its average ρ_0 to meet the demands of the membrane interior.[42] Incorporating R14 into $GW^{4,20}ALP23$ introduces an interaction between the Arg side chain and the lipid membrane that is strong enough to drastically limit the rotational averaging about ρ_0, exemplified by the massive drop in σ_ρ from 122° to 10° in DOPC, essentially locking the transmembrane helix into place. In spite of the arginine dominance, the competition between the two Trp residues remains, such that W20 likely causes additional C-terminal residues to unravel from the core helix (Figure 4), in order to obtain a preferential orientation for the W20 indole ring at the lipid/water interface. While residues A3 and A21 often are observed to unwind (see Figure 3),[23,24] now additional fraying of residues W20 and A19 is observed when R14 is present. By contrast, residue A3 near the N-terminal now fits to the central helix of $R^{14}GW^{4,20}ALP23$, indicating a shifting of the midpoint of the core helix. The N-terminus is likely compensating for the unwinding at the other end of the helix (see Figure 10 for a model).
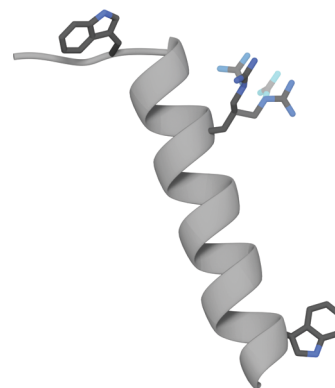

Figure 10. 3D model of $R^{14}GW^{4,20}ALP23$. A selection of possible arginine rotamers from the set in ref 94 is illustrated as potentially "snorkeling" toward the membrane interface. The C-terminal unwinding begins at residue A19.

Influence of R12. Placing the Arg residue (R12) at the center of GWALP23 sequences with varying locations for the outer Trp residues has interesting consequences. The peptide $R^{12}W^{5,19}ALP23$ produces ^2H NMR spectra with multiple states for every alanine residue in DOPC bilayers. According to molecular dynamics simulations, it adopts three primary states of which two are transmembrane and one is at the membrane surface.[14] When the tryptophans are moved outward by two residues each, $R^{12}W^{3,21}ALP23$ has ample room to accommodate R12 between the outer Trp residues.[16] The helix with W3 and W21 is able to remain transmembrane by adopting large tilt angles (24−30°) to accommodate the snorkeling of

R12 toward the surface of DOPC, DMPC, or DLPC bilayers, without interference from the aromatic side chains.

Introducing a small amount of cholesterol (10 mol %) was enough to drive $R^{12}GW^{5,19}$ALP23 completely to the surface of DOPC bilayers.[15] Similarly, H12 and K12 both drive $GW^{5,19}$ALP23 to the membrane surface, at low pH when H12 or K12 is positively charged.[8,9] Here, $R^{12}GW^{4,20}$ALP23 adopts a single overall orientation perpendicular to the DOPC bilayer normal, yet unlike the previous peptides, $R^{12}GW^{4,20}$ALP23 is distorted when bound on the membrane surface. The distortion is apparent from (a) the NMR resonance doubling of A9 and (b) the N-terminal residues preceding A9 not fitting to the same quadrupolar wave plot as the rest of the helix on the C-terminal side of A9 (Figures 6−8). The resonance doubling of A9 is likely observed because the helix actually starts to distort at residue A11, next to the central Arg at position 12. Thus, A9 is found, with about equal probability, within both the N-terminal and C-terminal helical segments. While residue A11 gives only one major ^{2}H NMR signal, additional minor peaks may be evident (Figure 6), although we are unable to assign specific minor peaks. Interestingly, and seemingly by coincidence, the major ^{2}H $|\Delta\nu_q|$ value for A11 fits both the N-terminal 3_{10}-helix and the C-terminal α-helix (Figure 7). While R14 caused unwinding of the $R^{14}GW^{4,20}$ALP23 helix at A19 (see above), the larger and more central distortion with R12 likely also is caused by the competing Trp residues W4 and W20, while the Arg again dominates the peptide dynamics. The C-terminal helix exhibits $\sigma\rho$ of 12°−25°, significantly lower than the parent helix when Arg is absent (Table 4). We note that the CD spectra (Figure 4B) are not particularly sensitive to the helix distortion revealed by the ^{2}H and ^{15}N NMR spectra.

As noted, it is likely that the $R^{12}GW^{4,20}$ALP23 helix on the DOPC membrane surface contains a 3_{10}-helical segment as well as an α-helical segment. The ^{2}H quadrupolar splittings of the C-terminal alanines fit only to an α-helix. Fitting the ^{2}H quadrupolar splittings of the N-terminal alanines to an α-helix is not possible, nevertheless, even in combination with the ^{15}N data (Table 4). On the other hand, a tighter 3_{10}-helix predicts a surface bound N-terminal segment with only a 40° difference in azimuthal rotation from the C-terminal helix. The rotational difference and the tighter N-terminal 3_{10}-helix then would allow the W20 side chain to reside at the membrane interface, oriented toward the lipids (see Figure 11), instead of projecting out of the membrane as would have been dictated by an extension of the C-terminal α-helix. Indeed, the ^{15}N chemical shifts also discount the possibility of a trans-membrane orientation and are instead characteristic of an orientation perpendicular to the bilayer normal.[29,76] In a 3_{10}-helix, the carbonyl oxygens are more exposed, such that the folding of such a transmembrane structure is unfavorable due to the low dialectic of the bilayer interior.[66] On the membrane surface, nevertheless, a 3_{10}-helix becomes a reasonable motif for adjusting the relative radial locations of the side chains of W4 and W20, such that both of the indole rings can face the membrane interface (Figure 11B,C). We note as well that both the C-terminal α-helix and N-terminal 3_{10}-helix orientations are similar to the interfacial state among the multiple orientations for the $R^{12}GW^{5,19}$ALP23 helix (Figure 11A). Interestingly, the addition of 5% cholesterol to the DOPC membrane drives essentially all of the $R^{12}GW^{5,19}$ALP23 helix population to the membrane surface.[15] Moving the trypto-
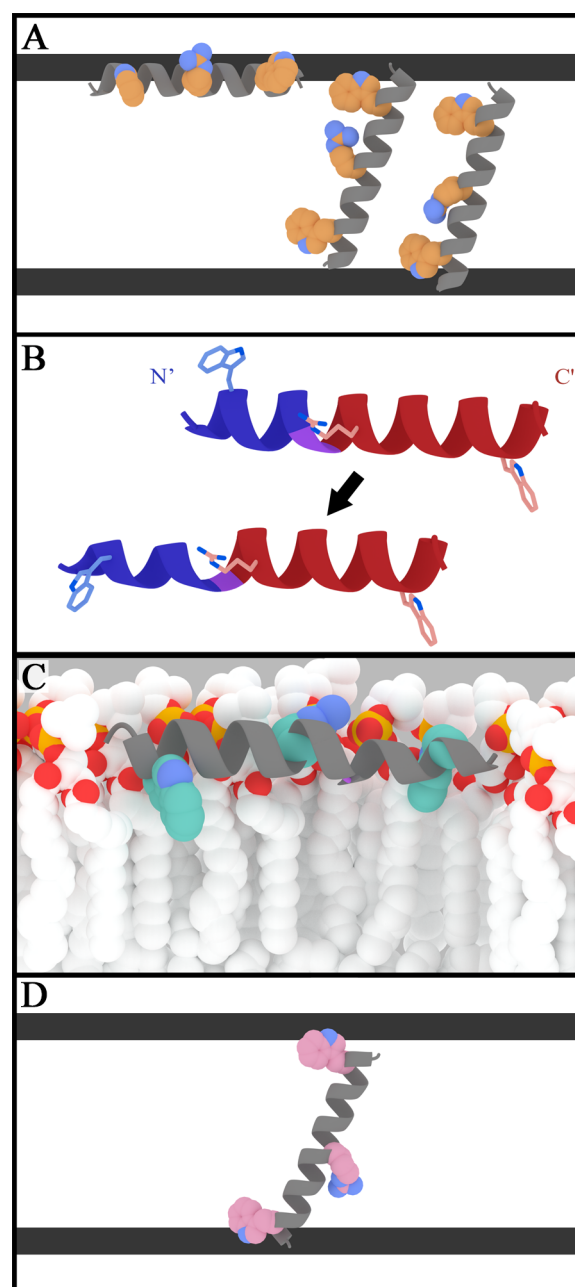

Figure 11. Models to illustrate the varying orientations, in DOPC bilayers, of 23-residue peptide helices with a central arginine residue, R12, and varying juxta-terminal tryptophans. (A) Multiple states observed, with about equal probabilities,[14] for the helix of $R^{12}GW^{5,19}$ALP23. The three states consist a surface helix and two transmembrane helices in which the R12 side chain snorkels either up or down.[14] (B) Distortion of the surface-bound helix of $R^{12}GW^{4,20}$ALP23 to yield a 3_{10}-helical segment (blue) for the N-terminal, based on the NMR evidence in Figures 7 and 8. (C) A model with lipids and the hybrid alpha(left)-3_{10}(right) helix of $R^{12}GW^{4,20}$ALP23, rotated 180° from the view in panel B. (D) Illustration of the stable transmembrane helix of $R^{12}GW^{3,21}$ALP23,[16] wherein the interfacial tryptophans are moved outward and away from the central R12 residue.

phans outward to positions 3 and 21, nevertheless, retains a tilted transmembrane helix (Figure 11D.)[16]

The ^{15}N separated local field experiments are in full support of a surface-bound helix, yet essentially show little sensitivity to the geometric differences between an α-helix or 3_{10}-helix at this

orientation. The insensitivity is largely because the plane perpendicular to the magnetic field/bilayer normal is additionally a reflection plane for the resonance frequencies[29,87] resulting in overlapping PISA wheel arcs over a small range of $^1H-^{15}N$ dipolar couplings and ^{15}N chemical shifts, which are both further reduced by motional averaging. The ^2H experiments span a much wider frequency range $(0-50$ kHz)[15,88] for surface bound helices and are therefore more sensitive in distinguishing the particular type of helix. The distinction would be easier for a transmembrane oriented peptide, as α-helices and 3_{10}-helices aligned on a plane parallel to the magnetic field each produce a distinctive PISA wheel pattern.[76] Indeed there are precedents for an Arg-rich motif containing an α-helix that kinks into a 3_{10}-helix, for example in the voltage sensing domains of membrane channel proteins.[89−92] A model for such a helix transition may be manifest here.

CONCLUSIONS

Incorporating one central Arg residue into the highly dynamic GW^{4,20}ALP23 helix framework has led to unique consequences. Placing Arg at position 14 arrests the dynamics, reorients the helix, and causes the C-terminal residues around W20 to unwind from the helix, probably to optimize the interfacial interactions of residue W20. By contrast, an Arg residue at position 12 brings the entire helix to the surface of DOPC bilayer membranes and distorts the helix so that residues 3−11 form a 3_{10}-helix while residues 9−19 remain α-helical, with deuterated Ala-9 itself giving two distinct ^2H NMR spectral signals that represent both of the helix motifs.

ASSOCIATED CONTENT

ⓢ Supporting Information

The Supporting Information is available free of charge on the ACS Publications website at DOI: 10.1021/acs.jpcb.9b06034.

Supplementary Figures S1−S5 (PDF)

AUTHOR INFORMATION

Corresponding Author
*E-mail: mjm035@uark.edu. Phone: 479-575-3181.

ORCID ⓘ
Matthew J. McKay: 0000-0002-3079-9189
Riqiang Fu: 0000-0003-0075-0410
Denise V. Greathouse: 0000-0001-7104-8499
Roger E. Koeppe, II: 0000-0003-0676-6413

Notes
The authors declare no competing financial interest.

REFERENCES

(1) Li, Q.; Wanderling, S.; Paduch, M.; Medovoy, D.; Singharoy, A.; McGreevy, R.; Villalba-Galea, C.; Hulse, R. E.; Roux, B.; Schulten, K.; Kossiakoff, A.; Perozo, E. Structural mechanism of voltage-dependent gating in an isolated voltage-sensing domain. *Nat. Struct. Mol. Biol.* **2014**, *21* (3), 244−252.

(2) Guo, J.; Zeng, W.; Chen, Q.; Lee, C.; Chen, L.; Yang, Y.; Cang, C.; Ren, D.; Jiang, Y. Structure of the voltage-gated two-pore channel TPC1 from Arabidopsis thaliana. *Nature* **2016**, *531*, 196.

(3) Killian, J. A.; von Heijne, G. How proteins adapt to a membrane−water interface. *Trends Biochem. Sci.* **2000**, *25* (9), 429−434.

(4) Mishra, V. K.; Palgunachari, M. N.; Segrest, J. P.; Anantharamaiah, G. M. Interactions of synthetic peptide analogs of the class A amphipathic helix with lipids. Evidence for the snorkel hypothesis. *J. Biol. Chem.* **1994**, *269* (10), 7185−7191.

(5) Tang, M.; Waring, A. J.; Hong, M. Phosphate-mediated arginine insertion into lipid membranes and pore formation by a cationic membrane peptide from solid-state NMR. *J. Am. Chem. Soc.* **2007**, *129* (37), 11438−11446.

(6) Doherty, T.; Su, Y.; Hong, M. High-resolution orientation and depth of insertion of the voltage-sensing S4 helix of a potassium channel in lipid bilayers. *J. Mol. Biol.* **2010**, *401* (4), 642−652.

(7) Vostrikov, V. V.; Grant, C. V.; Daily, A. E.; Opella, S. J.; Koeppe, R. E., II Comparison of "Polarization Inversion with Spin Exchange at Magic Angle" and "Geometric Analysis of Labeled Alanines" methods for transmembrane helix alignment. *J. Am. Chem. Soc.* **2008**, *130* (38), 12584.

(8) Gleason, N. J.; Vostrikov, V. V.; Greathouse, D. V.; Koeppe, R. E. Buried lysine, but not arginine, titrates and alters transmembrane helix tilt. *Proc. Natl. Acad. Sci. U. S. A.* **2013**, *110* (5), 1692−1695.

(9) Martfeld, A. N.; Greathouse, D. V.; Koeppe, R. E. Ionization properties of histidine residues in the lipid bilayer membrane environment. *J. Biol. Chem.* **2016**, *291* (36), 19146−19156.

(10) (a) Rajagopalan, R.; Greathouse, D. V.; Koeppe, R. E. Influence of glutamic acid residues and pH on the properties of transmembrane helices. *Biochim. Biophys. Acta, Biomembr.* **2017**, *1859*, 484−492. (b) Mortazavi, A.; Rajagopalan, V.; Sparks, K. A.; Greathouse, D. V.; Koeppe, R. E. Juxta-terminal helix unwinding as a stabilizing factor to modulate the dynamics of transmembrane helices. *ChemBioChem* **2016**, *17* (6), 462−465.

(11) Vostrikov, V. V.; Daily, A. E.; Greathouse, D. V.; Koeppe, R. E. Charged or aromatic anchor residue dependence of transmembrane peptide tilt. *J. Biol. Chem.* **2010**, *285* (41), 31723−31730.

(12) Killian, J. A.; Salemink, I.; dePlanque, M. R. R.; Lindblom, G.; Koeppe, R. E.; Greathouse, D. V. Induction of nonbilayer structures in diacylphosphatidylcholine model membranes by transmembrane alpha-helical peptides: Importance of hydrophobic mismatch and proposed role of tryptophans. *Biochemistry* **1996**, *35* (3), 1037−1045.

(13) Ramamoorthy, A.; Kandasamy, S. K.; Lee, D. K.; Kidambi, S.; Larson, R. G. Structure, topology, and tilt of cell-signaling peptides containing nuclear localization sequences in membrane bilayers determined by solid-state NMR and molecular dynamics simulation studies. *Biochemistry* **2007**, *46* (4), 965−975.

(14) Vostrikov, V. V.; Hall, B. A.; Greathouse, D. V.; Koeppe, R. E.; Sansom, M. S. P. Changes in transmembrane helix alignment by arginine residues revealed by solid-state nmr experiments and coarse-grained MD simulations. *J. Am. Chem. Soc.* **2010**, *132* (16), 5803−5811.

(15) Thibado, J. K.; Martfeld, A. N.; Greathouse, D. V.; Koeppe, R. E. Influence of high pH and cholesterol on single arginine-containing transmembrane peptide helices. *Biochemistry* **2016**, *55* (45), 6337−6343.

(16) Vostrikov, V. V.; Hall, B. A.; Sansom, M. S. P.; Koeppe, R. E. Accommodation of a central arginine in a transmembrane peptide by changing the placement of anchor residues. *J. Phys. Chem. B* **2012**, *116* (43), 12980−12990.

(17) Atkin, S. L.; Landolt, A. M.; Jeffreys, R. V.; Diver, M.; Radcliffe, J.; White, M. C. Basic fibroblastic growth-factor stimulates prolactin

secretion from human anterior-pituitary adenomas without affecting adenoma cell-proliferation. *J. Clin. Endocrinol. Metab.* **1993**, 77 (3), 831−837.

(18) Yamamoto, K.; Durr, U. H. N.; Xu, J. D.; Im, S. C.; Waskell, L.; Ramamoorthy, A. Dynamic interaction between membrane-bound full-length cytochrome P450 and cytochrome b(5) observed by solid-state NMR spectroscopy. *Sci. Rep.* **2013**, 3, 02538 DOI: 10.1038/srep02538.

(19) Litvinov, R. I.; Mravic, M.; Zhu, H.; Weisel, J. W.; DeGrado, W. F.; Bennett, J. S. Unique transmembrane domain interactions differentially modulate integrin alpha v beta 3 and alpha llb beta 3 function. *Proc. Natl. Acad. Sci. U. S. A.* **2019**, 116 (25), 12295−12300.

(20) Liu, D.; Angelova, A.; Liu, J. W.; Garamus, V. M.; Angelov, B.; Zhang, X. L.; Li, Y. W.; Feger, G.; Li, N.; Zou, A. H. Self-assembly of mitochondria-specific peptide amphiphiles amplifying lung cancer cell death through targeting the VDAC1-hexokinase-II complex. *J. Mater. Chem. B* **2019**, 7 (30), 4706−4716.

(21) MacKenzie, K. R. Folding and stability of alpha-helical integral membrane proteins. *Chem. Rev.* **2006**, 106 (5), 1931−1977.

(22) Cymer, F.; von Heijne, G.; White, S. H. Mechanisms of integral membrane protein insertion and folding. *J. Mol. Biol.* **2015**, 427 (5), 999−1022.

(23) McKay, M. J.; Afrose, F.; Koeppe, R. E.; Greathouse, D. V., Helix formation and stability in membranes. *Biochim. Biophys. Acta, Biomembr.* **2018**.18602108

(24) Afrose, F.; McKay, M. J.; Mortazavi, A.; Suresh Kumar, V.; Greathouse, D. V.; Koeppe, R. E. Transmembrane helix integrity versus fraying to expose hydrogen bonds at a membrane−water Interface. *Biochemistry* **2019**, 58 (6), 633−645.

(25) van der Wel, P. C. A.; Strandberg, E.; Killian, J. A.; Koeppe, R. E. Geometry and intrinsic tilt of a tryptophan-anchored trans-membrane alpha-helix determined by 2H NMR. *Biophys. J.* **2002**, 83 (3), 1479−1488.

(26) Strandberg, E.; Özdirekcan, S.; Rijkers, D. T. S.; van der Wel, P. C. A.; Koeppe, R. E.; Liskamp, R. M. J.; Killian, J. A. Tilt angles of transmembrane model peptides in oriented and non-oriented lipid bilayers as determined by H-2 solid-state NMR. *Biophys. J.* **2004**, 86 (6), 3709−3721.

(27) Strandberg, E.; Esteban-Martin, S.; Ulrich, A. S.; Salgado, J. Hydrophobic mismatch of mobile transmembrane helices: Merging theory and experiments. *Biochim. Biophys. Acta, Biomembr.* **2012**, 1818 (5), 1242−1249.

(28) Sparks, K. A.; Gleason, N. J.; Gist, R.; Langston, R.; Greathouse, D. V.; Koeppe, R. E. Comparisons of interfacial phe, tyr, and trp residues as determinants of orientation and dynamics for GWALP transmembrane peptides. *Biochemistry* **2014**, 53 (22), 3637−3645.

(29) Marassi, F. M.; Opella, S. J. A solid-state NMR index of helical membrane protein structure and topology. *J. Magn. Reson.* **2000**, 144 (1), 150−155.

(30) Wang, J.; Denny, J.; Tian, C.; Kim, S.; Mo, Y.; Kovacs, F.; Song, Z.; Nishimura, K.; Gan, Z.; Fu, R.; Quine, J. R.; Cross, T. A. Imaging membrane protein helical wheels. *J. Magn. Reson.* **2000**, 144 (1), 162−167.

(31) Opella, S. J.; Marassi, F. M. Applications of NMR to membrane proteins. *Arch. Biochem. Biophys.* **2017**, 628, 92−101.

(32) Ladizhansky, V. Applications of solid-state NMR to membrane proteins. *Biochim. Biophys. Acta, Proteins Proteomics* **2017**, 1865 (11), 1577−1586.

(33) Park, S. H.; Mrse, A. A.; Nevzorov, A. A.; Mesleh, M. F.; Oblatt-Montal, M.; Montal, M.; Opella, S. J. Three-dimensional structure of the channel-forming trans-membrane domain of virus protein ″u″ (Vpu) from HIV-1. *J. Mol. Biol.* **2003**, 333 (2), 409−424.

(34) Park, S. H.; Das, B. B.; Casagrande, F.; Tian, Y.; Nothnagel, H. J.; Chu, M.; Kiefer, H.; Maier, K.; De Angelis, A. A.; Marassi, F. M.; Opella, S. J. Structure of the chemokine receptor CXCR1 in phospholipid bilayers. *Nature* **2012**, 491 (7426), 779.

(35) Verardi, R.; Shi, L.; Traaseth, N. J.; Walsh, N.; Veglia, G. Structural topology of phospholamban pentamer in lipid bilayers by a hybrid solution and solid-state NMR method. *Proc. Natl. Acad. Sci. U. S. A.* **2011**, 108 (22), 9101−9106.

(36) Huang, R.; Yamamoto, K.; Zhang, M.; Popovych, N.; Hung, I.; Im, S. C.; Gan, Z. H.; Waskell, L.; Ramamoorthy, A. Probing the transmembrane structure and dynamics of microsomal NADPH-cytochrome P450 oxidoreductase by solid-state NMR. *Biophys. J.* **2014**, 106 (10), 2126−2133.

(37) Durr, U. H. N.; Yamamoto, K.; Im, S.-C.; Waskell, L.; Ramamoorthy, A. Solid-state NMR reveals structural and dynamical properties of a membrane-anchored electron-carrier protein, cyto-chrome b(5). *J. Am. Chem. Soc.* **2007**, 129 (21), 6670.

(38) Yamamoto, K.; Gildenberg, M.; Ahuja, S.; Im, S. C.; Pearcy, P.; Waskell, L.; Ramamoorthy, A. Probing the transmembrane structure and topology of microsomal cytochrome-P450 by solid-state NMR on temperature-resistant bicelles. *Sci. Rep.* **2013**, 3, 02556.

(39) Yamamoto, K.; Caporini, M. A.; Im, S. C.; Waskell, L.; Ramamoorthy, A. Transmembrane interactions of full-length mammalian bitopic cytochrome-P450-cytochrome-b(5) complex in lipid bilayers revealed by sensitivity-enhanced dynamic nuclear polarization solid-state NMR spectroscopy. *Sci. Rep.* **2017**, 7, 04219-1 DOI: 10.1038/s41598-017-04219-1.

(40) Sharma, M.; Yi, M.; Dong, H.; Qin, H.; Peterson, E.; Busath, D. D.; Zhou, H.-X.; Cross, T. A. Insight into the mechanism of the influenza a proton channel from a structure in a lipid bilayer. *Science* **2010**, 330 (6003), 509−512.

(41) Das, N.; Dai, J.; Hung, I.; Rajagopalan, M. R.; Zhou, H.-X.; Cross, T. A. Structure of CrgA, a cell division structural and regulatory protein from Mycobacterium tuberculosis, in lipid bilayers. *Proc. Natl. Acad. Sci. U. S. A.* **2015**, 112 (2), E119−E126.

(42) McKay, M. J.; Martfeld, A. N.; De Angelis, A. A.; Opella, S. J.; Greathouse, D. V.; Koeppe, R. E. Control of transmembrane helix dynamics by interfacial tryptophan residues. *Biophys. J.* **2018**, 114 (11), 2617−2629.

(43) Kulandaisamy, A.; Priya, S. B.; Sakthivel, R.; Frishman, D.; Gromiha, M. M. Statistical analysis of disease-causing and neutral mutations in human membrane proteins. *Proteins: Struct., Funct., Genet.* **2019**, 87 (6), 452−466.

(44) Nastou, K. C.; Batskinis, M. A.; Litou, Z. I.; Hamodrakas, S. J.; Iconomidou, V. A. Analysis of single-nucleotide polymorphisms in human voltage-gated ion channels. *J. Proteome Res.* **2019**, 18 (5), 2310−2320.

(45) Catterall, W. Sodium channel structure and function at atomic resolution. *Biophys. J.* **2012**, 102 (3), 7a−8a.

(46) Sula, A.; Wallace, B. A. Interpreting the functional role of a novel interaction motif in prokaryotic sodium channels. *J. Gen. Physiol.* **2017**, 149 (6), 613−622.

(47) Rotoli, B. M.; Barilli, A.; Ingoglia, F.; Visigalli, R.; Bianchi, M. G.; Ferrari, F.; Martinelli, D.; Dionisi-Vici, C.; Dall'Asta, V. Analysis of LPI-causing mutations on y+LAT1 function and localization. *Orphanet Journal of Rare Diseases* **2019**, 14, 63 DOI: 10.1186/s13023-019-1028-2.

(48) Thomas, R.; Vostrikov, V. V.; Greathouse, D. V.; Koeppe, R. E. Influence of proline upon the folding and geometry of the WALP19 transmembrane peptide. *Biochemistry* **2009**, 48 (50), 11883−11891.

(49) Lobley, A.; Whitmore, L.; Wallace, B. A. DICHROWEB: an interactive website for the analysis of protein secondary structure from circular dichroism spectra. *Bioinformatics* **2002**, 18 (1), 211−212.

(50) Whitmore, L.; Wallace, B. A. DICHROWEB, an online server for protein secondary structure analyses from circular dichroism spectroscopic data. *Nucleic Acids Res.* **2004**, 32, W668−W673.

(51) Moll, F., 3rd; Cross, T. A. Optimizing and characterizing alignment of oriented lipid bilayers containing gramicidin D. *Biophys. J.* **1990**, 57 (2), 351−362.

(52) Hallock, K. J.; Henzler Wildman, K.; Lee, D.-K.; Ramamoorthy, A. An innovative procedure using a sublimable solid to align lipid bilayers for solid-state NMR studies. *Biophys. J.* **2002**, 82 (5), 2499−2503.

(53) Davis, J. H.; Jeffrey, K. R.; Bloom, M.; Valic, M. I.; Higgs, T. P. Quadrupolar echo deuteron magnetic-resonance spectroscopy in

ordered hydrocarbon chains. *Chem. Phys. Lett.* **1976**, *42* (2), 390−394.

(54) Nevzorov, A. A.; Opella, S. J. Selective averaging for high-resolution solid-state NMR spectroscopy of aligned samples. *J. Magn. Reson.* **2007**, *185* (1), 59−70.

(55) Gor'kov, P. L.; Chekmenev, E. Y.; Li, C. G.; Cotten, M.; Buffy, J. J.; Traaseth, N. J.; Veglia, G.; Brey, W. W. Using low-E resonators to reduce RF heating in biological samples for static solid-state NMR up to 900 MHz. *J. Magn. Reson.* **2007**, *185* (1), 77−93.

(56) Levitt, M. H.; Suter, D.; Ernst, R. R. Spin dynamics and thermodynamics in solid-state NMR cross polarization. *J. Chem. Phys.* **1986**, *84* (8), 4243−4255.

(57) Fung, B.; Khitrin, A.; Ermolaev, K. An improved broadband decoupling sequence for liquid crystals and solids. *J. Magn. Reson.* **2000**, *142* (1), 97−101.

(58) Delaglio, F.; Grzesiek, S.; Vuister, G. W.; Zhu, G.; Pfeifer, J.; Bax, A. NMRPIPE - a multidimensional spectral processing system based on Unix pipes. *J. Biomol. NMR* **1995**, *6* (3), 277−293.

(59) Goddard, T. D.; Kneller, D. G. *SPARKY 3*; University of California: San Francisco.

(60) Wishart, D. S.; Bigam, C. G.; Yao, J.; Abildgaard, F.; Dyson, H. J.; Oldfield, E.; Markley, J. L.; Sykes, B. D. 1H, 13C and 15N chemical-shift referencing in biomolecular NMR. *J. Biomol. NMR* **1995**, *6* (2), 135−140.

(61) Enkhbayar, P.; Hikichi, K.; Osaki, M.; Kretsinger, R. H.; Matsushima, N. 3(10)-helices in proteins are parahelices. *Proteins: Struct., Funct., Genet.* **2006**, *64* (3), 691−699.

(62) Rosendaal, B. A.; Kuznetsov, A.; Nussbaumer, A.; Riakiotakis, A.; Skorupa, B.; Montagne, B.; et al. *Blender [computer program]*, version 2.79; Blender Foundation: Amsterdam, 1998.

(63) Pettersen EF, G. T.; Huang, C. C.; Couch, G. S.; Greenblatt, D. M.; Meng, E. C.; Ferrin, T. E. UCSF Chimera−a visualization system for exploratory research and analysis. *J. Comput. Chem.* **2004**, *25* (13), 1605−1612.

(64) Vostrikov, V. V.; Grant, C. V.; Opella, S. J.; Koeppe, R. E. On the combined analysis of 2H and 15N/1H solid-state NMR data for determination of transmembrane peptide orientation and dynamics. *Biophys. J.* **2011**, *101* (12), 2939−2947.

(65) Strandberg, E.; Esteban-Martin, S.; Salgado, J.; Ulrich, A. S. Orientation and dynamics of peptides in membranes calculated from 2H-NMR data. *Biophys. J.* **2009**, *96* (8), 3223−3232.

(66) Page, R. C.; Kim, S.; Cross, T. A. Transmembrane helix uniformity examined by spectral mapping of torsion angles. *Structure* **2008**, *16* (5), 787−797.

(67) Daily, A. E.; Greathouse, D. V.; van der Wel, P. C. A.; Koeppe, R. E. Helical distortion in tryptophan- and lysine-anchored membrane-spanning α-helices as a function of hydrophobic mismatch: a solid-state deuterium NMR investigation using the geometric analysis of labeled alanines method. *Biophys. J.* **2008**, *94* (2), 480−491.

(68) Provencher, S. W.; Glockner, J. Estimation of globular protein secondary structure from circular dichroism. *Biochemistry* **1981**, *20* (1), 33−37.

(69) Vanstokkum, I. H. M.; Spoelder, H. J. W.; Bloemendal, M.; Vangrondelle, R.; Groen, F. C. A. Estimation of protein secondary structure and error analysis from circular-dichroism spectra. *Anal. Biochem.* **1990**, *191* (1), 110−118.

(70) Andrade, M. A.; Chacon, P.; Merelo, J. J.; Moran, F. Evaluation of secondary structure of proteins from uv circular-dichroism spectra using an unsupervised learning neural-network. *Protein Eng., Des. Sel.* **1993**, *6* (4), 383−390.

(71) van der Wel, P. C. A.; Reed, N. D.; Greathouse, D. V.; Koeppe, R. E. Orientation and motion of tryptophan interfacial anchors in membrane-spanning peptides. *Biochemistry* **2007**, *46* (25), 7514−7524.

(72) Vieira-Pires, R. S.; Morais-Cabral, J. H. 310 helices in channels and other membrane proteins. *J. Gen. Physiol.* **2010**, *136* (6), 585−592.

(73) Payandeh, J.; Scheuer, T.; Zheng, N.; Catterall, W. A. The crystal structure of a voltage-gated sodium channel. *Nature* **2011**, *475*, 353.

(74) Zhang, X.; Ren, W.; DeCaen, P.; Yan, C.; Tao, X.; Tang, L.; Wang, J.; Hasegawa, K.; Kumasaka, T.; He, J.; Wang, J.; Clapham, D. E.; Yan, N. Crystal structure of an orthologue of the NaChBac voltage-gated sodium channel. *Nature* **2012**, *486*, 130.

(75) Pauling, L.; Corey, R. B.; Branson, H. R. The structure of proteins: Two hydrogen-bonded helical configurations of the polypeptide chain. *Proc. Natl. Acad. Sci. U. S. A.* **1951**, *37* (4), 205−211.

(76) Kim, S.; Cross, T. A. 2D solid state NMR spectral simulation of 310, α, and π-helices. *J. Magn. Reson.* **2004**, *168* (2), 187−193.

(77) Marassi, F. M.; Ma, C.; Gesell, J. J.; Opella, S. J. Three-dimensional solid-state NMR spectroscopy is essential for resolution of resonances from in-plane residues in uniformly N-15-labeled helical membrane proteins in oriented lipid bilayers. *J. Magn. Reson.* **2000**, *144* (1), 156−161.

(78) Traaseth, N. J.; Buffy, J. J.; Zamoon, J.; Veglia, G. Structural dynamics and topology of phospholamban in oriented lipid bilayers using multidimensional solid-state NMR. *Biochemistry* **2006**, *45* (46), 13827−13834.

(79) Opella, S. J.; Marassi, F. M. Structure determination of membrane proteins by NMR spectroscopy. *Chem. Rev.* **2004**, *104* (8), 3587−3606.

(80) Fitch, C. A.; Platzer, G.; Okon, M.; Garcia-Moreno, B.; McIntosh, L. P. Arginine: Its pK(a) value revisited. *Protein Sci.* **2015**, *24* (5), 752−761.

(81) Dorairaj, S.; Allen, T. W. On the thermodynamic stability of a charged arginine side chain in a transmembrane helix. *Proc. Natl. Acad. Sci. U. S. A.* **2007**, *104* (12), 4943−4948.

(82) Roux, B. Lonely arginine seeks friendly environment. *J. Gen. Physiol.* **2007**, *130* (2), 233−236.

(83) Li, L.; Vorobyov, I.; MacKerell, A. D.; Allen, T. W. Is arginine charged in a membrane? *Biophys. J.* **2008**, *94* (2), L11−L13.

(84) Harms, M. J.; Schlessman, J. L.; Sue, G. R.; Garcia-Moreno, B. Arginine residues at internal positions in a protein are always charged. *Proc. Natl. Acad. Sci. U. S. A.* **2011**, *108* (47), 18954−18959.

(85) Ulmschneider, J. P.; Smith, J. C.; White, S. H.; Ulmschneider, M. B. The importance of the membrane interface as the reference state for membrane protein stability. *Biochim. Biophys. Acta, Biomembr.* **2018**, *1860* (12), 2539−2548.

(86) Freites, J. A.; Tobias, D. J.; von Heijne, G.; White, S. H. Interface connections of a transmembrane voltage sensor. *Proc. Natl. Acad. Sci. U. S. A.* **2005**, *102* (42), 15059−15064.

(87) Murray, D. T.; Das, N.; Cross, T. A. Solid state NMR strategy for characterizing native membrane protein structures. *Acc. Chem. Res.* **2013**, *46* (9), 2172−2181.

(88) Strandberg, E.; Grau-Campistany, A.; Wadhwani, P.; Burck, J.; Rabanal, F.; Ulrich, A. S. Helix fraying and lipid-dependent structure of a short amphipathic membrane-bound peptide revealed by solid-state NMR. *J. Phys. Chem. B* **2018**, *122* (23), 6236−6250.

(89) Long, S. B.; Campbell, E. B.; MacKinnon, R. Crystal structure of a mammalian voltage-dependent shaker family K+ channel. *Science* **2005**, *309* (5736), 897−903.

(90) Long, S. B.; Tao, X.; Campbell, E. B.; MacKinnon, R. Atomic structure of a voltage-dependent K+ channel in a lipid membrane-like environment. *Nature* **2007**, *450* (7168), 376−U3.

(91) Clayton, G. M.; Altieri, S.; Heginbotham, L.; Unger, V. M.; Morais-Cabral, J. H. Structure of the transmembrane regions of a bacterial cyclic nucleotide-regulated channel. *Proc. Natl. Acad. Sci. U. S. A.* **2008**, *105* (5), 1511−1515.

(92) Schwaiger, C. S.; Bjelkmar, P.; Hess, B.; Lindahl, E. 3(10)-helix conformation facilitates the transition of a voltage sensor S4 segment toward the down state. *Biophys. J.* **2011**, *100* (6), 1446−1454.

(93) Esteban-Martin, S.; Strandberg, E.; Salgado, J.; Ulrich, A. Solid state NMR analysis of peptides in membranes: Influence of dynamics and labeling scheme. *Biochim. Biophys. Acta, Biomembr.* **2010**, *1798* (2), 252−257.

(94) Lovell, S. C.; Word, J. M.; Richardson, J. S.; Richardson, D. C. The penultimate rotamer library. *Proteins: Struct., Funct., Genet.* **2000**, *40* (3), 389−408.